UNIVERSITY OF MICHIGAN
Cavitation and Multiphase Flow Laboratory
Department of Mechanical Engineering

Report No. UMICH 014571-1-I

INVESTIGATION OF THE BEHAVIOR OF A THIN WAVY LIQUID FILM, AND THE STRUCTURE OF ITS DISINTEGRATED DROPLETS IN A CO-CURRENT STEAM FLOW

by

W. Kim

(Submitted in partial fulfillment of M.E. 990)

Approved by: F. G. Hammitt

Supported by: NSF Grant Nos. ENG 75-2315 and GK-40130

July, 1976

Table

Figures

I. INTRODUCTION

For the modern large powerplant, the behavior and stability of thin liquid films on the turbine blades under high velocity steam flow and their subsequent break-up into liquid droplets, which are then entrained into the wake and give rise to an erosion problem in the next downstream rotating row, have come to the attention of many researchers. They are considered to be the important economic factor. Besides the particular application of the steam turbine, liquid film behavior and stability has many applications in the modern technology society. The conveying of liquids by co-current gas streams in oil pipelines, boiler tubes and heat transfer from wavy films of molten material on spacecraft are examples. Along these lines of interest, a wet steam tunnel has been designed, constructed and tested at the University of Michigan (1-5).

The low pressure steam tunnel can produce an approximately sonic velocity (450 m/sec) in a rectangular test section (8 cm x 8 cm) at the pressure of 3 psia (20.67×10^3 N $/m^2$). Simulated turbine blades, i.e., essentially thin flat plates, are inserted parallel to the flow direction along the axis of the test section. A liquid film thickness measurement technique using electrical conductivity gages has been developed and calibrated (2,3). The behavior of liquid films, under adiabatic and diabatic conditions, has been studied elsewhere (5).

In this paper, I am interested in the liquid film stability, especially regarding the wave patterns appearing at the interface

between liquid film and steam, and the structure and behavior of the liquid droplets disintegrated at the trailing edge of the fixed blade due to aerodynamic forces. The droplets thus formed are believed to be about 4 orders of magnitude larger than the primary droplets due to condensation in the wet steam.

I have measured the wavelength and thickness of the liquid film on the blade and the size and distribution of droplets in the downstream flow under diabatic condition for various steam and liquid flow rates.

II. EXPERIMENTAL FACILITY AND CONDITION

Figure 1 shows a schematic diagram of our steam tunnel facility. The test section is composed of a horizontal rectangular plexiglass with the blade (Fig. 3) inserted parallel to the stream. Steam is flowing through a stilling tank into the test section and through a diffuser to a jet-cooled condenser.

As discussed in Ref. 5, the flow rate of steam is measured by an upstream orifice rather than pitot tube, because of its possible contribution to turbulence in the downstream flow.

The liquid film is formed by supplying the liquid through a slot in the blade instead of by direct condensing of the steam. The liquid flow rate is measured by a conventional flow meter. The liquid film thickness was measured by the electrical conductivity gages. The liquid film wavelengths and droplet sizes are measured by high-speed camera pictures (Fig. 2). An E.G.&G strobe flash tube was used as a light source. Oscilloscope camera pictures, which provide film

thickness and frequency information, were taken simultaneously with high-speed camera pictures, by connecting a syncronization unit between the two cameras.

The range of this investigation is characterized by the following conditions:

$(P_3)_{max}$; 3.75 psia (0.258×10^5 N/m^2): Saturated steam

P_4 2.55 psia (0.175×10^5 N/m^2)

Steam Velocity: 50 m (M= 0.13) to 300 m/sec (M= 0.75)

Liquid Flow Rate: 0.32 Cm^3/min Cm to 12.5 Cm^3/min. Cm.

Mean Film Thickness: 20 μm to 220 μm.

Wave Length: symmetric wave 0.5 mm to 2.5 mm
non-symmetric wave 5 mm to 10 mm

Camera Picture Magification: 2.4

Light Flash Duration: 1 μs

Droplet size; 50 μm and larger.

III. RESULTS OF FILM OBSERVATION

By direct observation of numerous high-speed camera pictures (about 350), four kinds of liquid film patterns have been discerned:

a. Dry patches
b. Symmetric waves
c. Non-symmetric cluster waves
d. Film break up

A map of these transition patterns is presented in Fig. 10.

For a constant steam velocity, dry patches are first seen at a small liquid flow rate (Fig. 3, 1 of Fig. 10). Minimum film thickness measurements for dry patch formation is important for nuclear reactor emergency core cooling techniques. A theoretical approach for predicting dry patch formation was

developed by Mikielewicz and Moszynski (7).

At slightly larger liquid flow rates, small symmetrical waves appear. (Fig. 5, 2 of Fig. 10). The wave lengths of those waves are 1 -2.5 mm. The wave fronts are almost straight and perpendicular to the direction of flow. As the liquid flow rate increases the wave lengths tend to decrease (Fig. 11).

At still larger flow rates, the regular symmetrical waves tend to become less regular and the wave cross section assumes the non-symmetrical shape of a cluster with a steep front and a long tail (Fig. 7, 4 of Fig. 10).

Usually each such "cluster-wave" is preceded by a number of small satellite wavelets which move as a group with the main waves. The wave length of this cluster wave was $\sim$ 5 to 10 mm, and that of the proceding wavelets $\sim$ 0.3-0.4 mm.

The wave length of the cluster waves becomes smaller as the flow rate increases (Fig. 11). In this regime of flow the wave fronts show a tendency to form bulges or to split, or to overtake each other.

Comparing the wave lengths of symmetric and non-symmetric waves, an increase is noted for the non-symmetric wave regime i.e., by a factor of 6.3 Standard deviation σ , gives the measure of randomness for the wave lengths in both regimes. Wave lengths are more scattered in the non-symmetric wave region by x 10 i.e., $\sigma_{\text{non-sym}} = 10 \times \sigma_{\text{sym}}$. See Table 1. As the liquid flow rate increases, a stage is reached where the main waves and their individual wave fronts can hardly be

distinguished and the surface breaks and sheds into the main steam flow. (Fig. 7 and 5 of Fig. 10).

This transition line from regime 4 to 5 is compared to the results of other investigations where gas flow is air (Fig. 13 and Ref. 6) while ours was of course steam.

The steam-liquid film is torn when it was $\sim$ 0.2 x thickness and 7 times the gas phase velocity found in the air-liquid film case.

4. SECONDARY LIQUID DROPLETS STRUCTURE IN STEAM WAKE

The film is broken at the wave crests at moderately high liquid flow rates and high steam velocity (Fig. 7). However, most of the secondary droplets detected in the downstream of the blade are those which disintegrated at the trailing edge of the blade (Fig. 8). The maximum droplet size which has been estimated based on the theoretical approach (8) for the last stage of the turbine was about 300 μm. Other authors (9,10) expected droplets larger than 1 mm. Experimental turbines were used for that research. Using high speed camera, droplet sizes cannot be measured less than 50 μm. For the erosion problem in the steam turbine, the larger droplets are always of most importance. However, a method to measure the droplet size less than 50 μm has other technical applications. For example, in the internal combustion engine, the fuel burns in the state of liquid droplets ($\sim$ 5-15 μm) instead of the gaseous state. The distribution of these smaller droplets is considered to be an important design factor for internal combustion engines. The laser scattering method is expected

to solve this smaller size measurement problem.

Many photographs have been taken in the present study at three Mach numbers:

$M = 0.35,\ 0.55,\ 0.75$ and at

three values of the flow rate.

$q = 2.5,\ 5.0\quad 10\ \ Cm^3/Cm \times min.$

These are presented in Figs. 14-16. All the data points are provided as a function of distance downstream in the aerodynamic wake (x-coordinate). The relationship between maximum droplet size and distance downstream, $D_{max} = f(x)$ is established as a limiting line above the area of the data points. The function $D_{max} = f(x)$ decreases with distance for $x \leqq 20$ Cm and then remains essentially constant. Variation of D_{max} does not depend on liquid flow rate for this experiment. However the shape of the curves depends very strong on Mach number (Fig. 17).

From this data, $We_{max} = f(M)$ is obtained, where

$$We_{max} = \frac{\rho V_\infty^{\,2} D_{max}}{\sigma}$$

D_{max}; maximum droplet size, at distance x = 22 Cm, assuming maximum droplet size to be approximately constant for distances longer than x = 22 Cm.

V_∞ ; the velocity of steam

σ ; surface tension at the given temperature

ρ ; density of liquid

This result is compared to others (Fig. 18) i.e., Weigle and Severin (11) using an air tunnel and Valha from a steam tunnel(12). In order to obtain more information about droplet stream structure, droplet size distribution function has been proposed.

The function is defined:

$$F(d) = \frac{N(d)}{N} \cdot \frac{1}{\Delta d}$$

d; average droplet size

Δd; droplet size interval (Δd = 200 μm) in this case

N(d); average number of droplets of the size enclosed the region $\left(d - \frac{\Delta d}{2},\ d + \frac{\Delta d}{2} \right)$

N; average total number of the droplets visible in the test area.

Droplet Mass Distribution Function , R(m), is defined from f(d):

$$R(m) = \frac{m(d)}{m} \frac{1}{\Delta d} = \frac{d_i^3 \cdot N(d_i)}{\sum_{i=1}^{n} d_i^3 N(d_i)} \frac{1}{\Delta d} = \frac{d_i^3 f(d_i)}{\sum_{i=1}^{n} d_i^3 f(d_i)} \frac{1}{\Delta d}$$

m(d) = average mass of droplets of the size enclosed in the region $\left(d - \frac{\Delta d}{2},\ d + \frac{\Delta d}{2}\right)$

m = average total mass of the droplets visible in the test area.

$n = \frac{d_{max}}{\Delta d}$

Both functions were normalized in order for the integral to be unity. The size and mass distribution functions are shown in Figs. 19-22 for M = 0.35; M = 0.55. The size and mass distribution functions of large droplets decreases while those of small droplets increase as the distance x increases.

5. CONCLUSIONS

The objects of this investigation were the behavior of injected thin films of water under the effect of steam flow, and the structure of droplets in the downstream wake which were disintegrated at the trailing edge of the blade.

1. A plot of wave lengths under different steam flow and liquid flow conditions indicates that wave lengths decrease as liquid flow rates increase, but increase as steam velocities decrease.

2. The mean wave length and standard deviations are listed (T1). This gives the measure of randomness of the wave lengths in symmetric and non-symmetric waves.

3. A "transition map" for steam liquid film is presented. Compared with an air-liquid film transition map previously published (6), it is found that our steam-liquid film flow is broken and torn away at less thickness and higher steam velocities than was observed for the air-water studies. The mechanism of the transition lines will be the subject of future study.

4. The maximum droplet size function $D_{max} = g(x,M)$, decreases with the distance x and Mach number M. D_{max} becomes constant for x - 22 Cm. In this region, maximum droplet size varies with Mach number.

$M = 0.35 : D_{max} = 750$ um

$0.55 : \quad = 500$ um

$0.75 : \quad = 250$ um

5. The critical value of the Weber number $We = \frac{\rho V_\infty^2 D_{max}}{\sigma}$ has been estimated as follows:

M = .035; We = 30

M = .055, 0.75, We = 45 (Fig. 18)

6. The most probable droplet size to appear in the aerodynamic wake, at the vicinity of the trailing edge (x = 2.5 to 4 Cm), according to the size distribution function is

M = 0.35; d = 375 μm
M = 0.55; d = 175 μm

and according to the mass distribution function is:

M = 0.35; d = 750 μm
M = 0.55; d = 740 μm

7. There is no significant influence of liquid flow rate on the maximum droplet size D_{max} and on the droplet size and mass distribution function f(d), R(m).

ACKNOWLEDGMENT

The author is indebted to Prof. F. G. Hammitt and Dr. S. Krzeczkowski for their consistent advise and guidance. Also the support from NSF Grant No. ENG 75-2315 and GK 40130 is greatly appreciated.

References

1. J. Krzyzanowski, "Wet-Steam Tunnel Facility - Design and Program of Investigations," ORA Report No. UMICH 03371-18-T, June 1972.

2. J. Mikielewicz, F.G. Hammitt, "Generalized Characteristics of Electrical Conductance Film Thickness Gauges," ORA Report No. UMICH 012449-7-I, December 1974; to be published Trans. IFFM, PAN, Gdansk, Poland.

3. F.G. Hammitt, J. Mikielewicz, G. Ernst, "Steam Tunnel Initial Operation and Results," ORA Report No. UMICH 012449-6-T, January 1975.

4. S. Krzeczkowski, W. Kim, F.G. Hammitt, J-B. Hwang, "Investigations of Secondary Liquid Phase Structure in Steam Wake," ORA Report No. UMICH 014571-1-T, June 1976; submitted Trans. ASME, J. Fluids Engr., ASME.

5. F.G. Hammitt, J-B. Hwang, etal., "Liquid Film Thickness Tests - Wet Steam Tunnel," ORA Report No. UMICH 012449-9-T, June 1975.

6. D. Wurz, "Flow Behavior of Thin Water Films Under the Effect of a Co-current Air Flow of Moderate to High Subsonic Velocities," Proc. of the Third International Conf. on Rain Erosion and Associated Phenomena, ed. A.A. Fyall, Elvetham Hall, England, Aug. 11-13, 1970, p. 727-750.

7. J. Mikielewicz, J.R. Moszynski, "Shear Driven Liquid Film," Trans. IFFM, PAN, 66, 1975, Gdansk, Poland, p. 3-10.

8. R. Puzyrewski, S. Krezeczkowski, "Some Results of Investigations on Water-Film Breakup and Motion of Water Drops in Aerodynamic Trail," IFFM Trans., Gdansk, Poland, 1966, p. 29-31.

9. D.G. Christie, G.W. Haywood, "Observation of Events Leading to the Formation of Water Drops Which Cause Turbine Blade Erosion," Phil. Trans. Roy. Soc., 260 SA, no. 1110, London, 1966.

10. J.P. Faddeev, "Structure of Erosion Inducing Streams of Droplets in Axial Clearance of Low-Pressure Part of Turbine," Proc. of the III Conf. on Steam Turbines of Great Output, Prace IMP-PAN, Gdansk, Poland, 1975.

11. B. Weigle, H. Severin, "Badania nad wplywem predkosci fazy gazowej na strukture strumienia kropel i jego oddzialywanie na efekty erozji," IFFM Bulletin, Nr arch. 273/71, Gdansk, 1971.

12. J. Valha, "Liquid Film Disintegration on the Trailing Edges of Swept Bodies," Strojnicky Časopis, Ročnik XXI, čislo 3, 1970.

Table 1 The Average Wave Lengths and Standard Deviation

V_s	Symmetric		Non-Symmetric	
m/s	$\bar{\lambda}$ mm	σ	$\bar{\lambda}$ mm	σ
54.3	1.92	0.380	8.48	0.84
79.3	1.28	0.0834	7.40	1.66
129.6	1.36	0.0940	7.14	1.31
220.5	0.573	0.0310	5.65	1.60
302			4.21	1.38

$\bar{\lambda}$; Mean Value of Wave Length

σ ; Standard Deviation of Each Wave Length

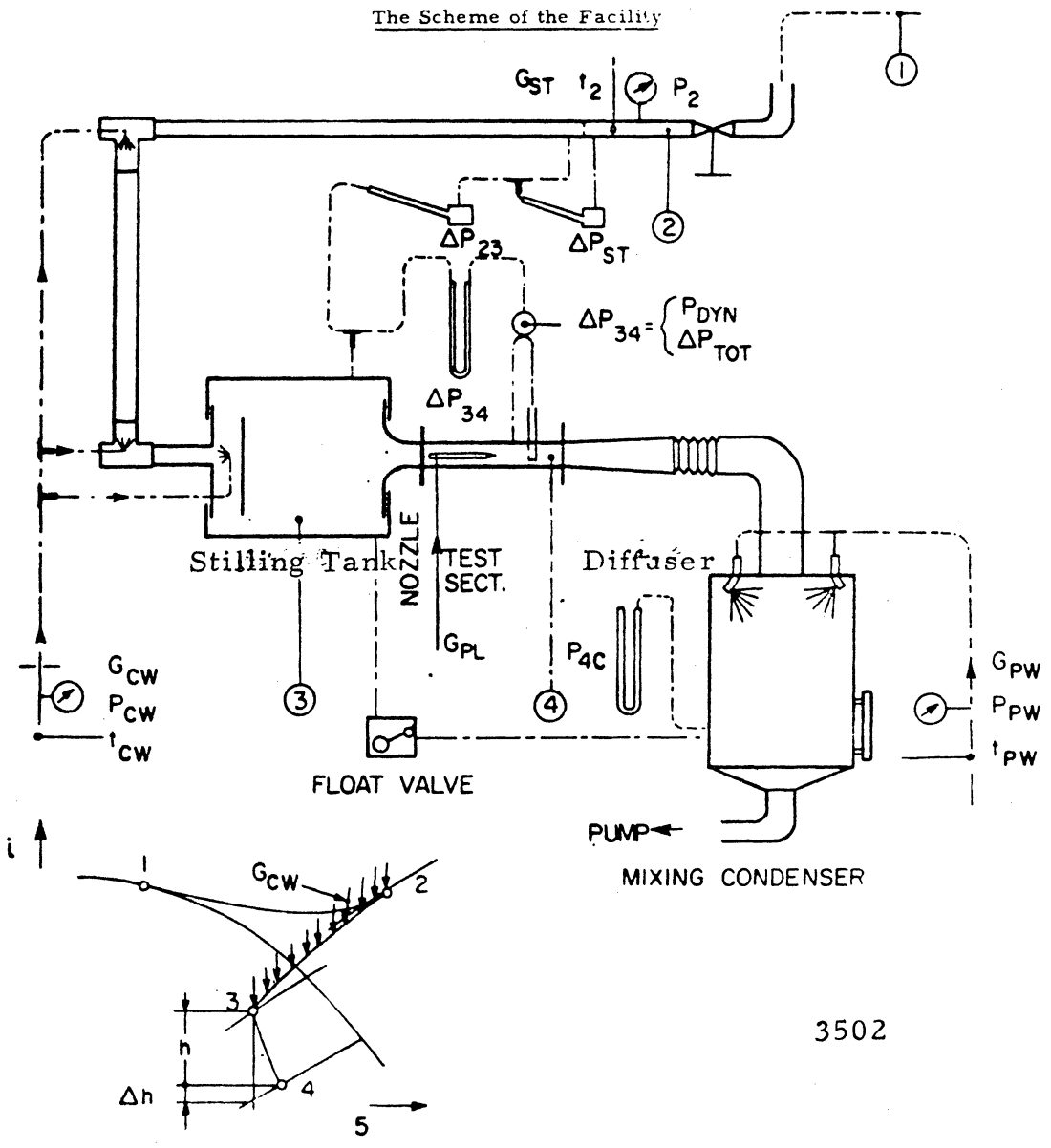

Fig. 1 Schematic of Steam Tunnel Facility

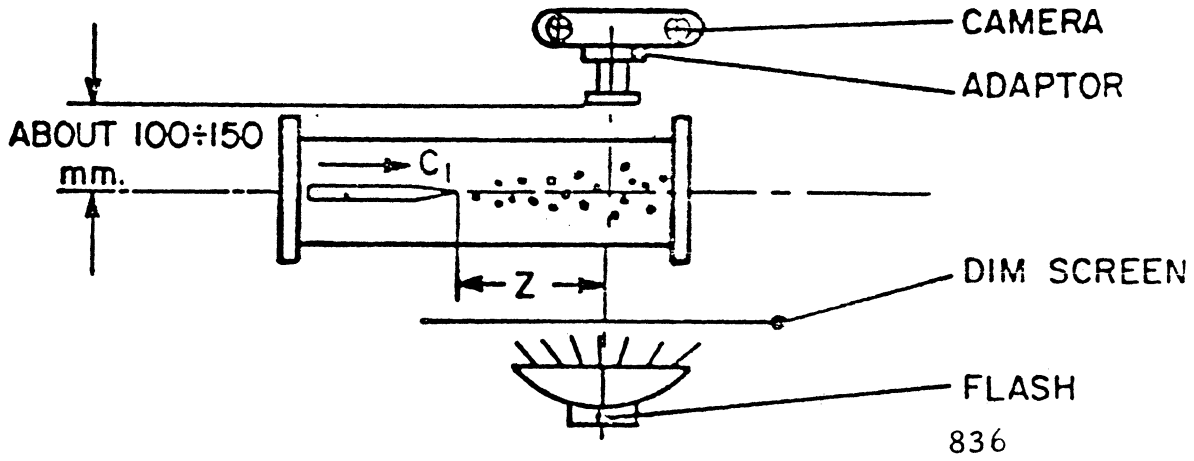

Figure 2 - Schematic of Test Section and the Position of Camera and Flash (4)

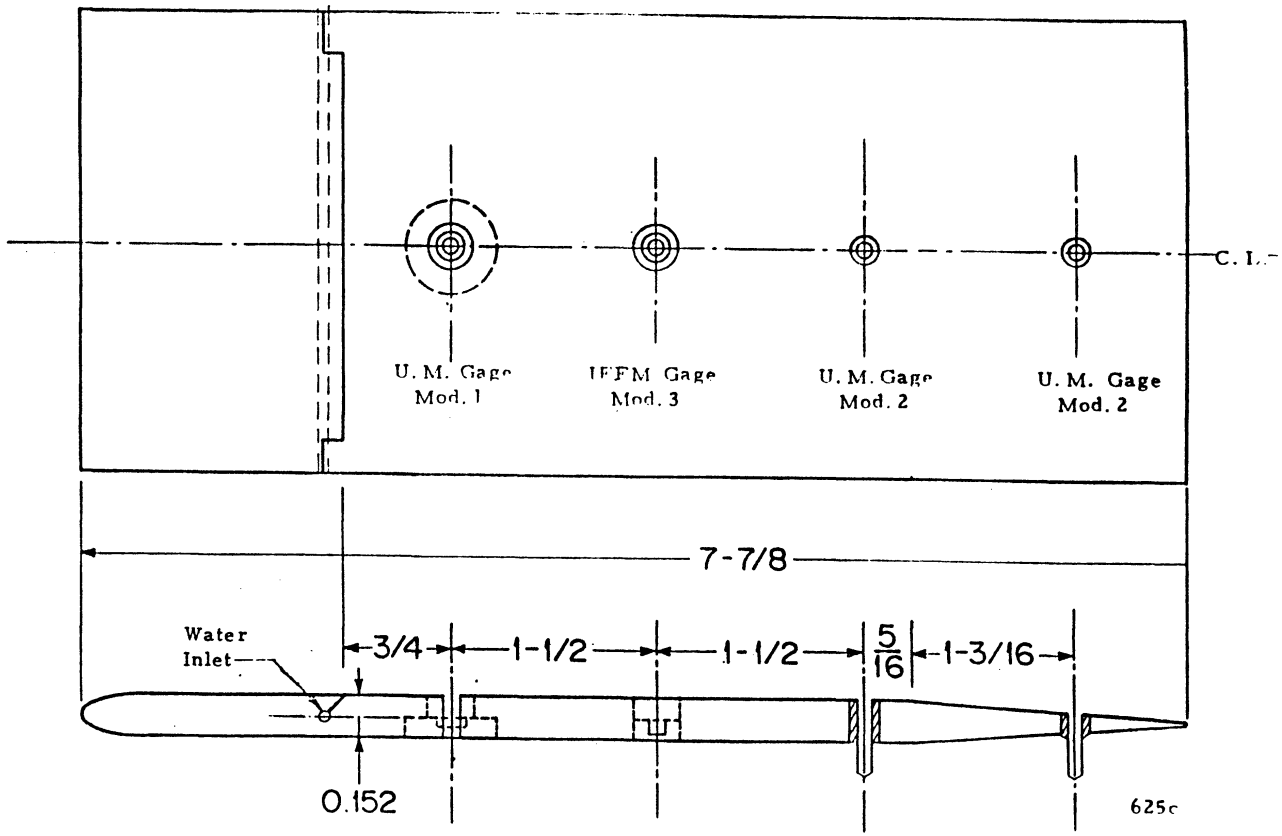

Figure 3 - Schematic of Blade with Gages

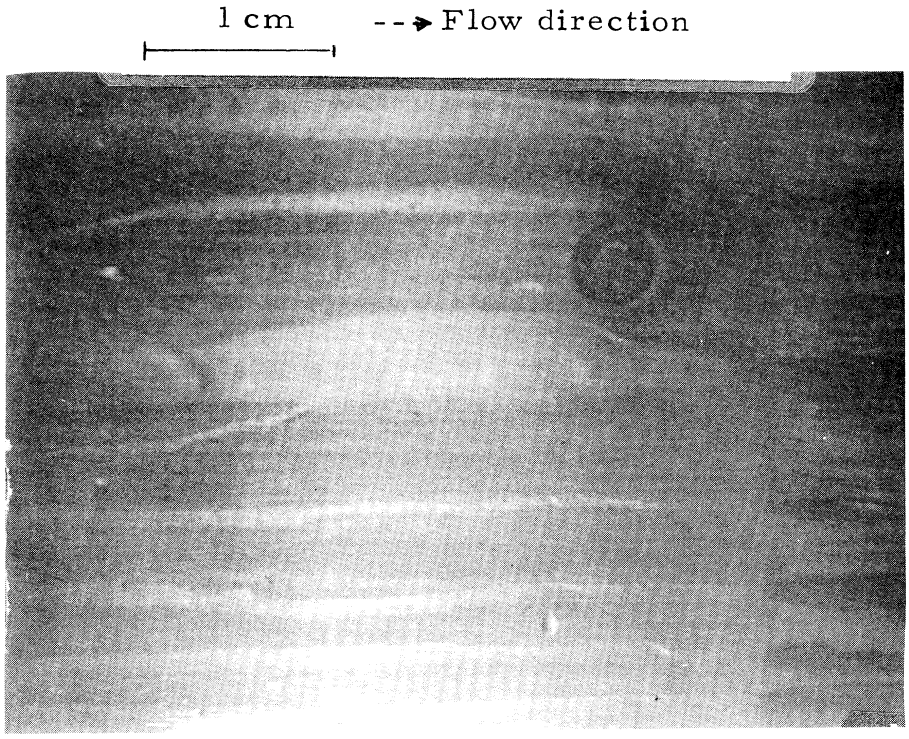

853a

4. Dry Patch , V_s = 79 m/s, $\dot{q}$ = 5/8 Cm^3/min Cm

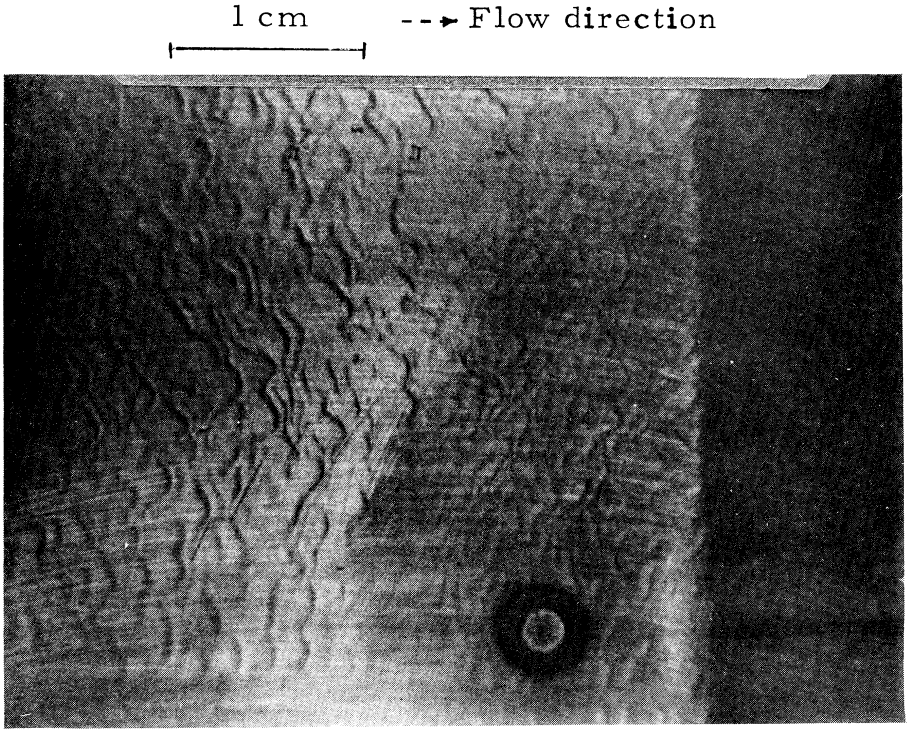

853b

5. Symmetric Wave, V_s = 130 m/s, $\dot{q}$ = 15/16 Cm^3/min Cm

1 cm ---→Flow direction

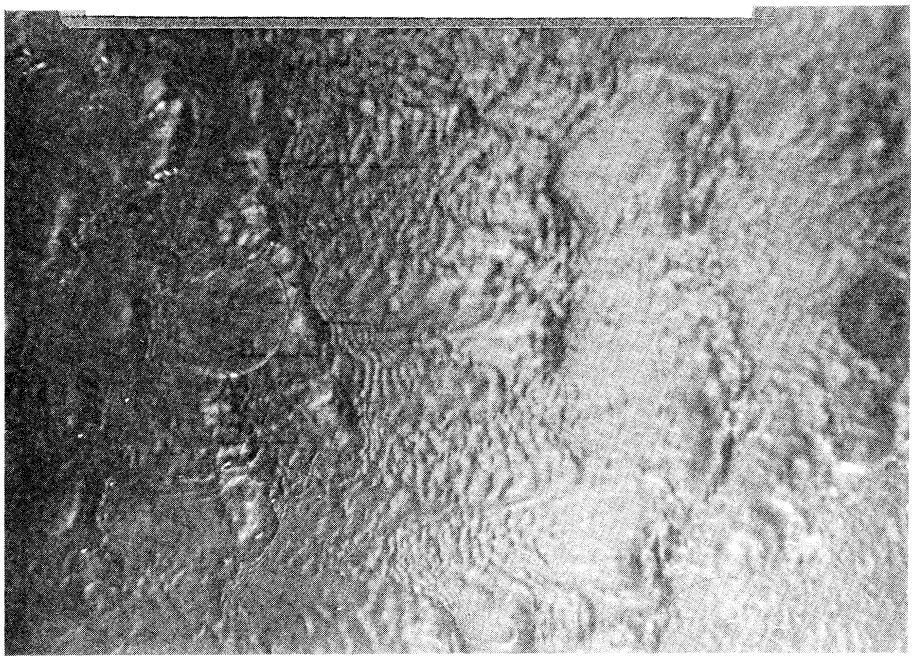

6. Non-Symmetric Wave, V_s = 54 m/s, $\tilde{q}$ = 7.5 Cm^3/Cm-min

1 cm ---➤Flow direction

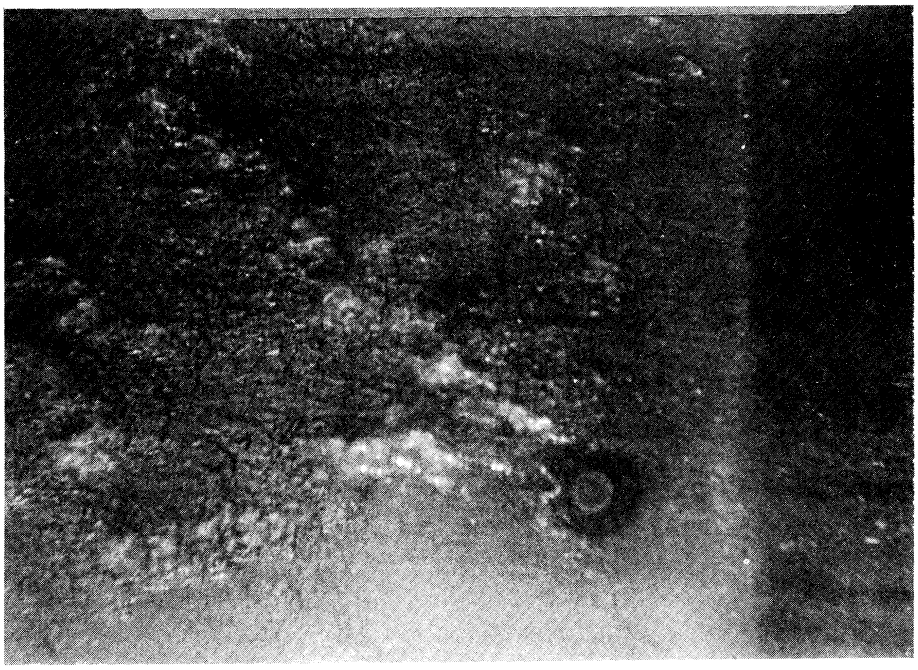

7. Film Break Up and Shedding, V_s = 302 m/s, $\dot{q}$ = /2.5 Cm^3/min Cm

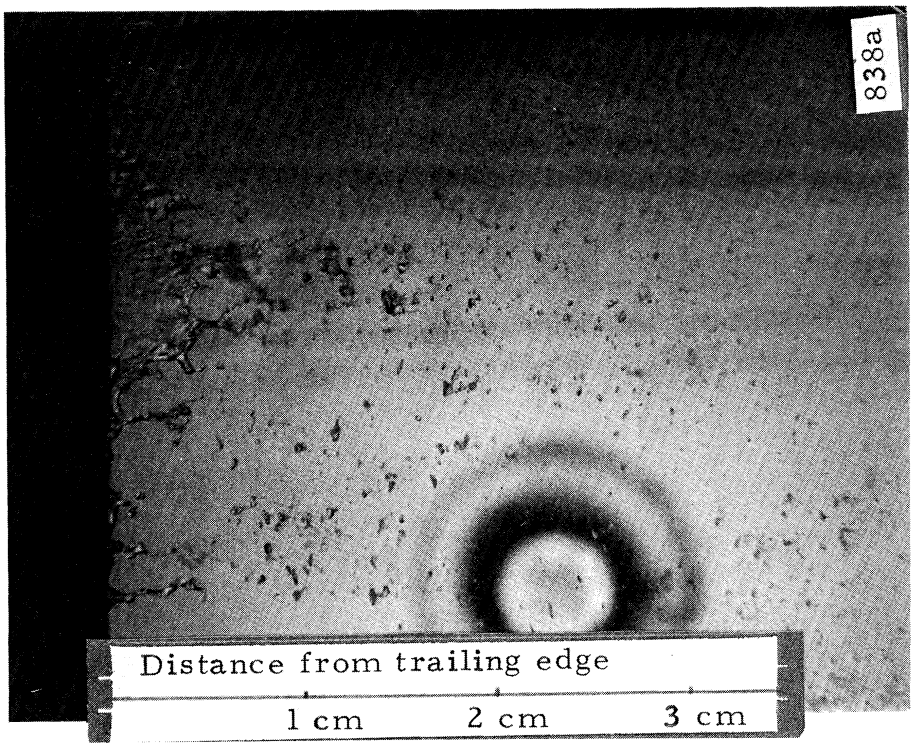

8. Liquid Film Disintegration, V_s = 302 m/s (M = 0.75), $\hat{q}$ = 5 Cm^3/min Cm

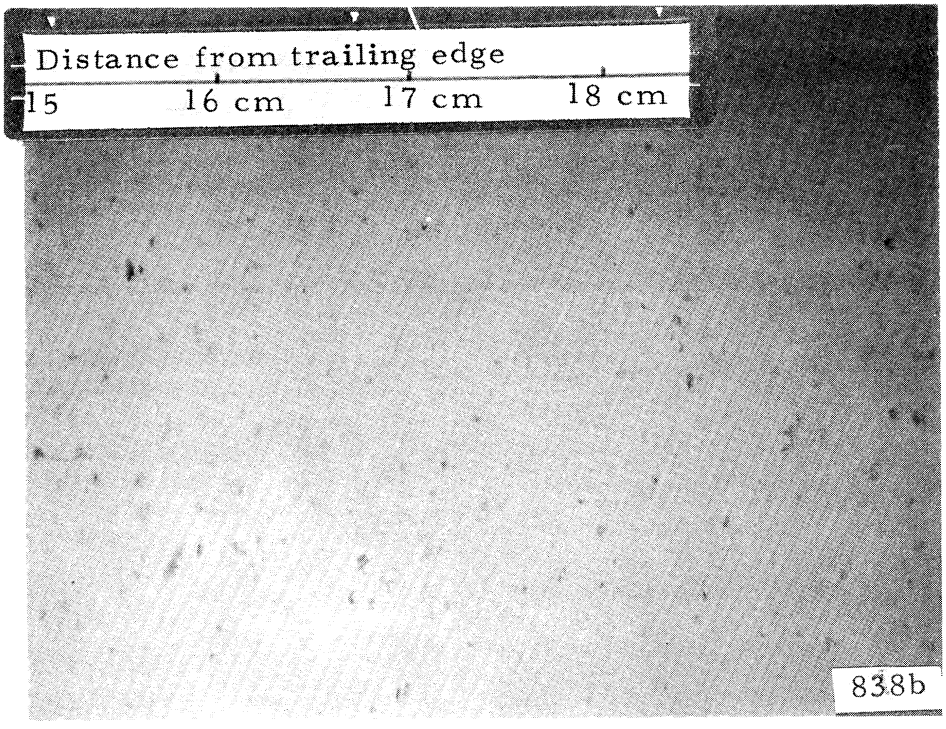

9. Liquid Droplets Disintegration, V_s = 130 m/s (M = 0.35), $\hat{q}$ = 10 Cm^3/min Cm, x = 15 Cm

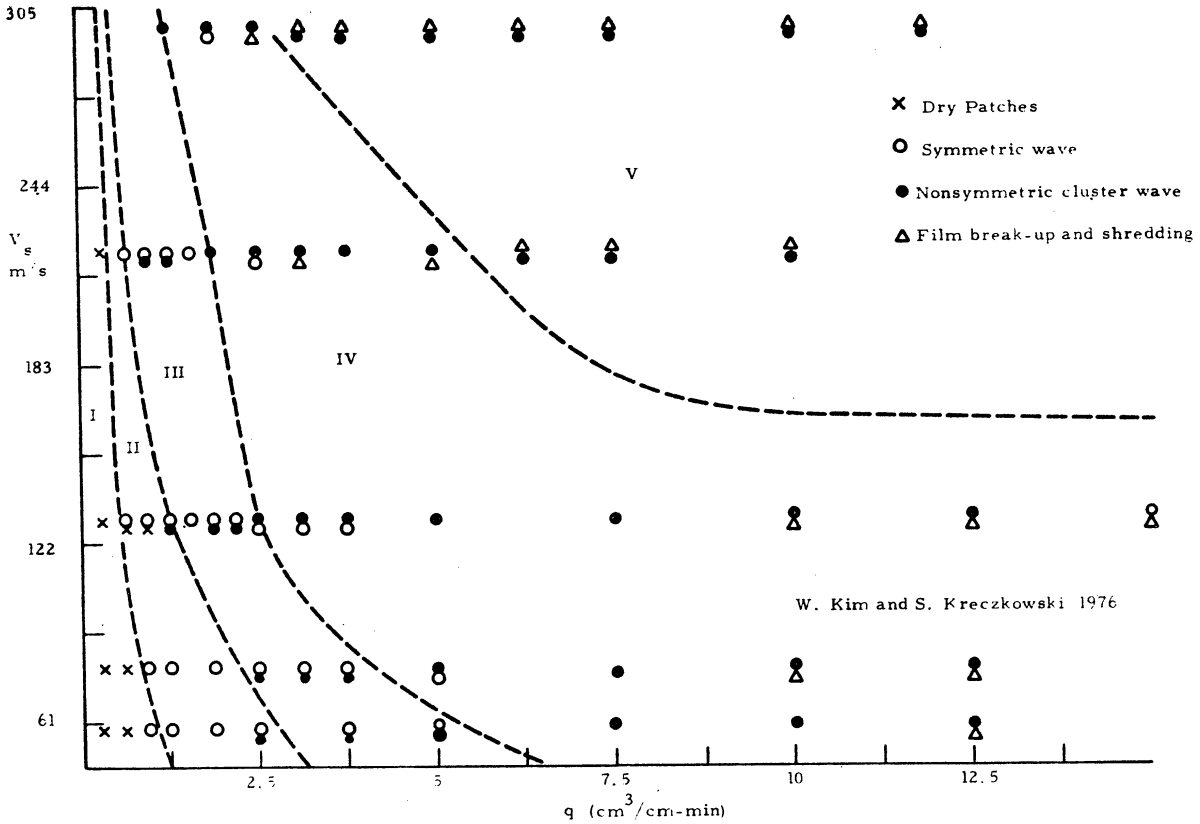

Fig. 10 Transition Map of Liquid Film and Steam Flow

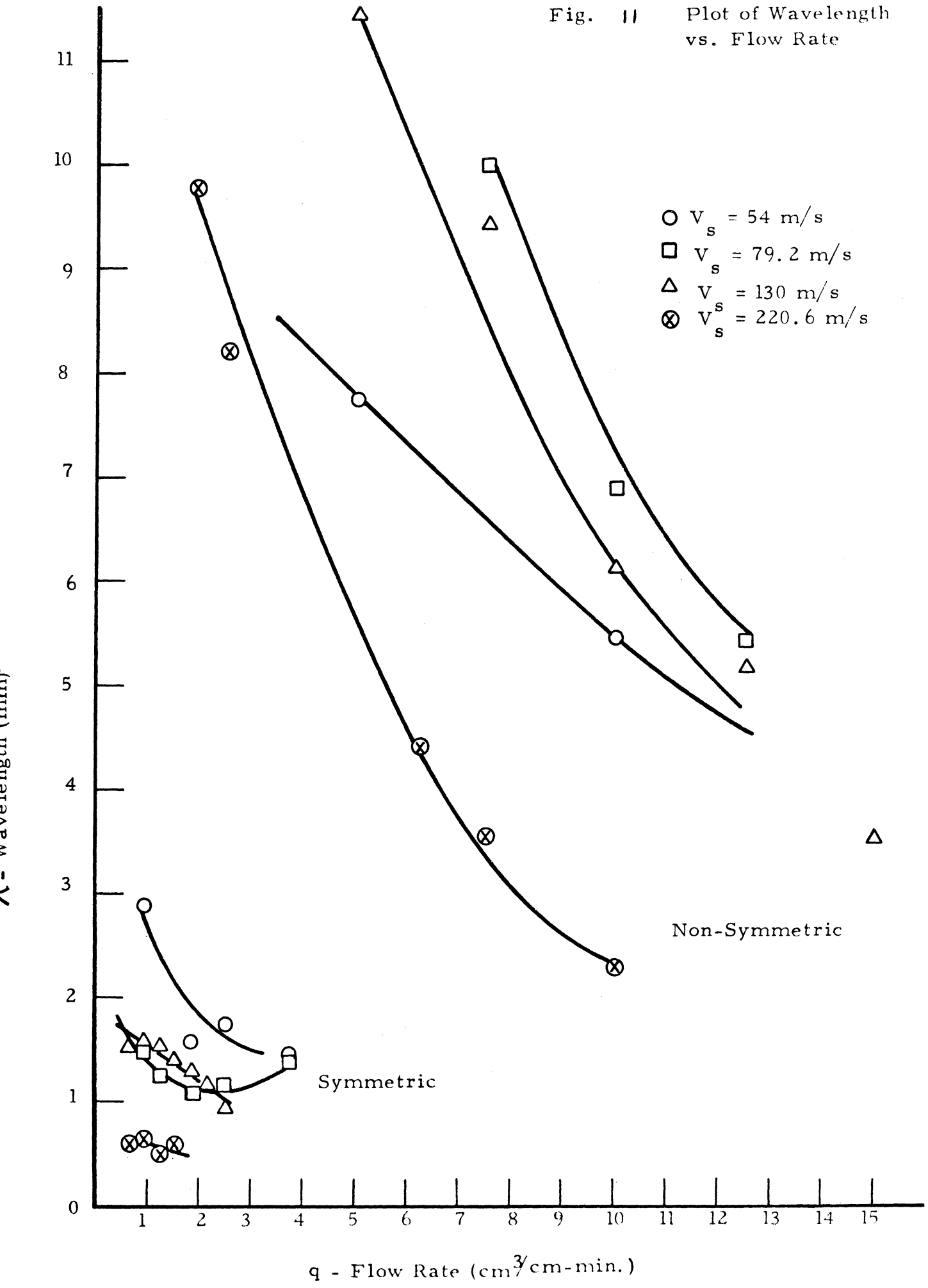
Fig. 11 Plot of Wavelength vs. Flow Rate
V_s = 54 m/s
V_s = 79.2 m/s
V_s = 130 m/s
V_s = 220.6 m/s
Non-Symmetric
Symmetric
λ - Wavelength (mm)
q - Flow Rate (cm^3/cm-min.)
0
1
2
3
4
5
6
7
8
9
10
11
12
13
14
15

Fig. 12 Plot of Dimensionless Wavelength vs. Reynold's Number

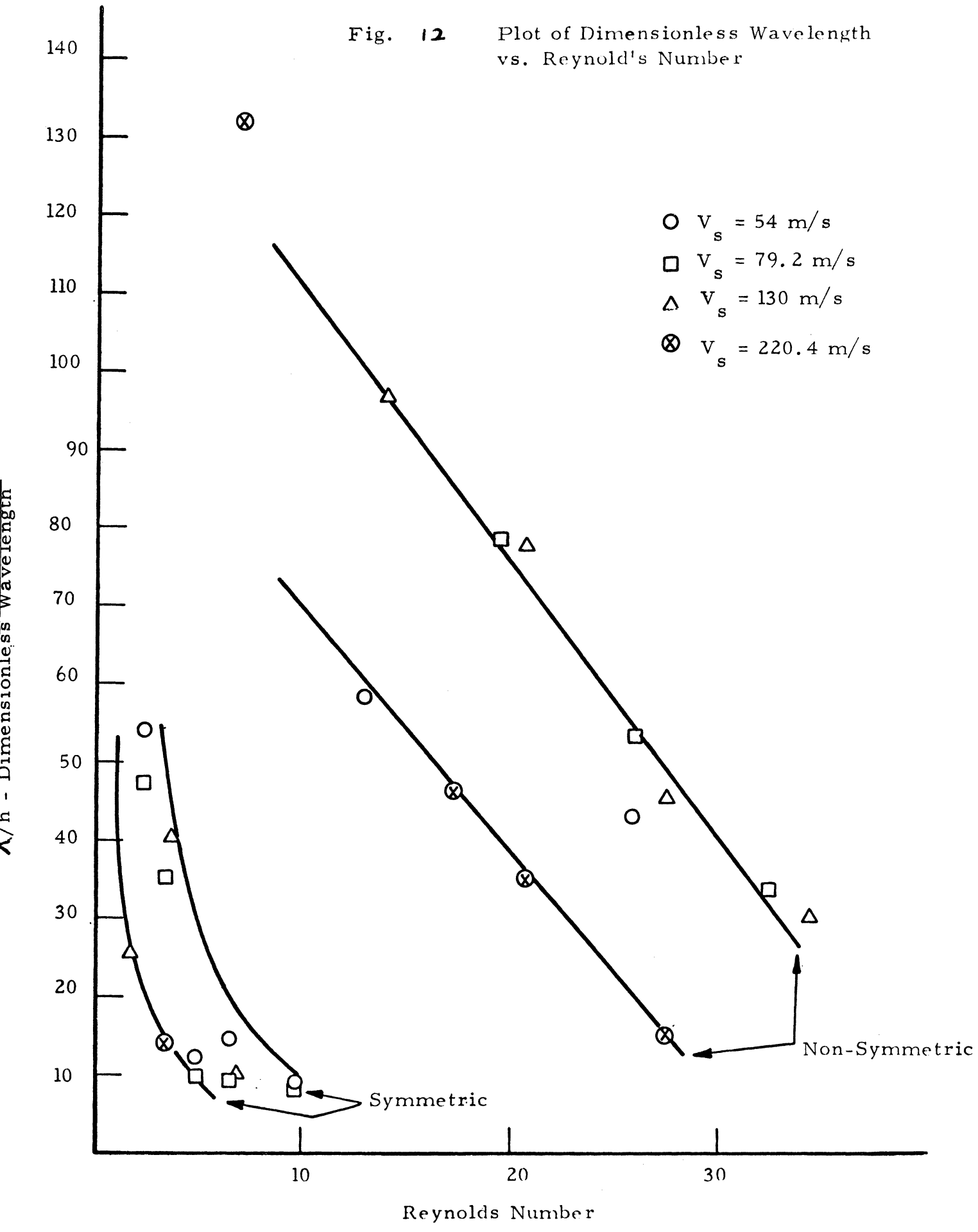

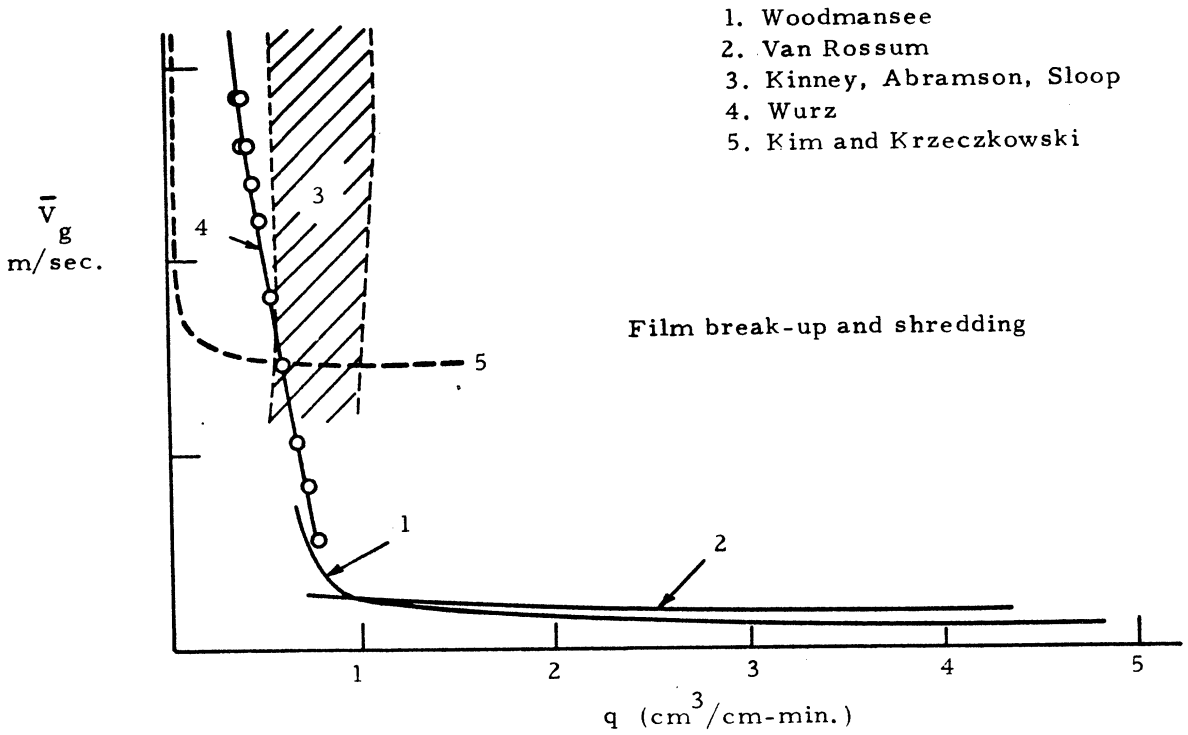

Fig. 13 Transition Line for Film Break-up

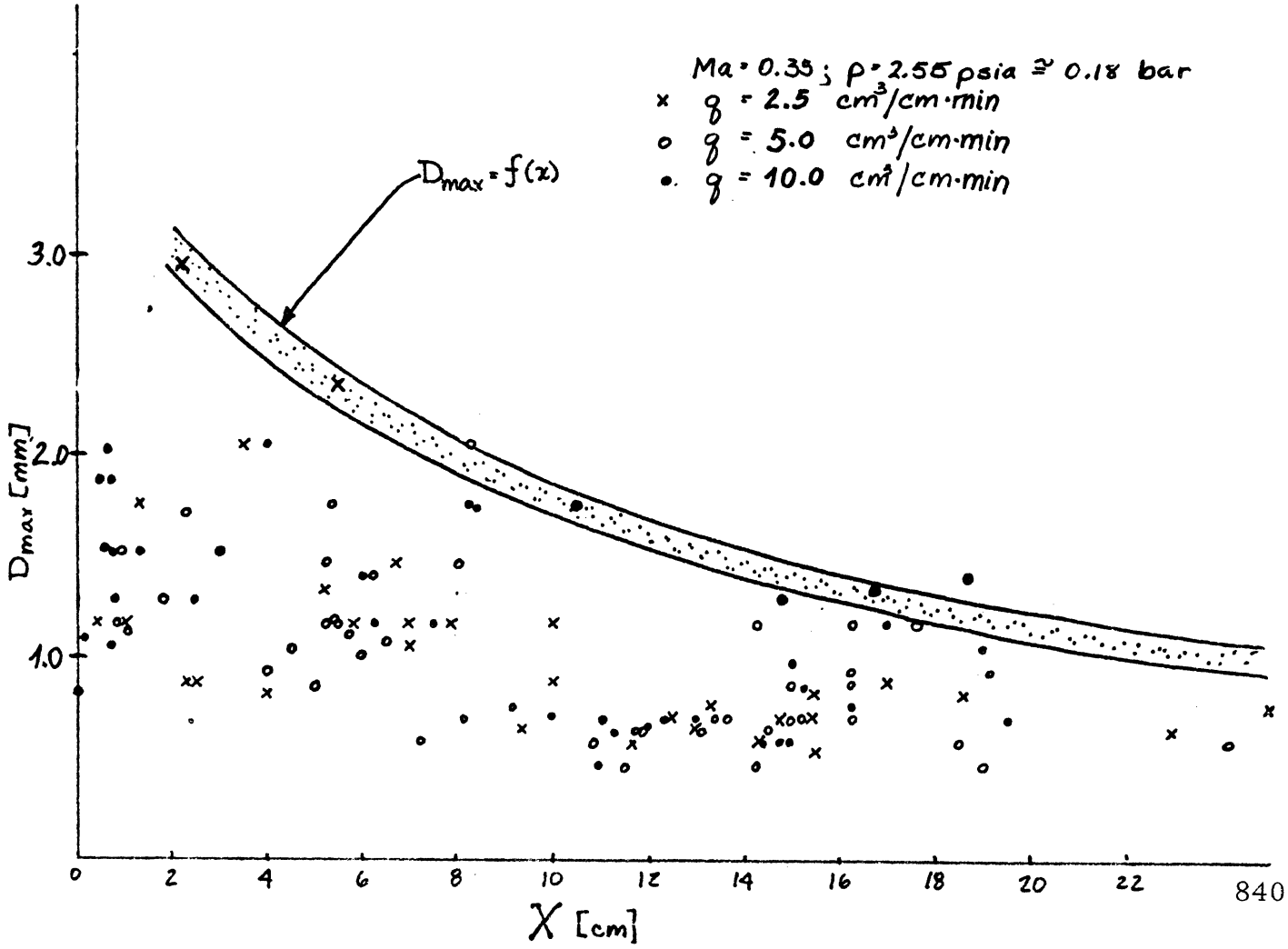

Figure 14 - Maximum Droplet Size as a Function of the Distance From the Trailing Edge, M = 0.35

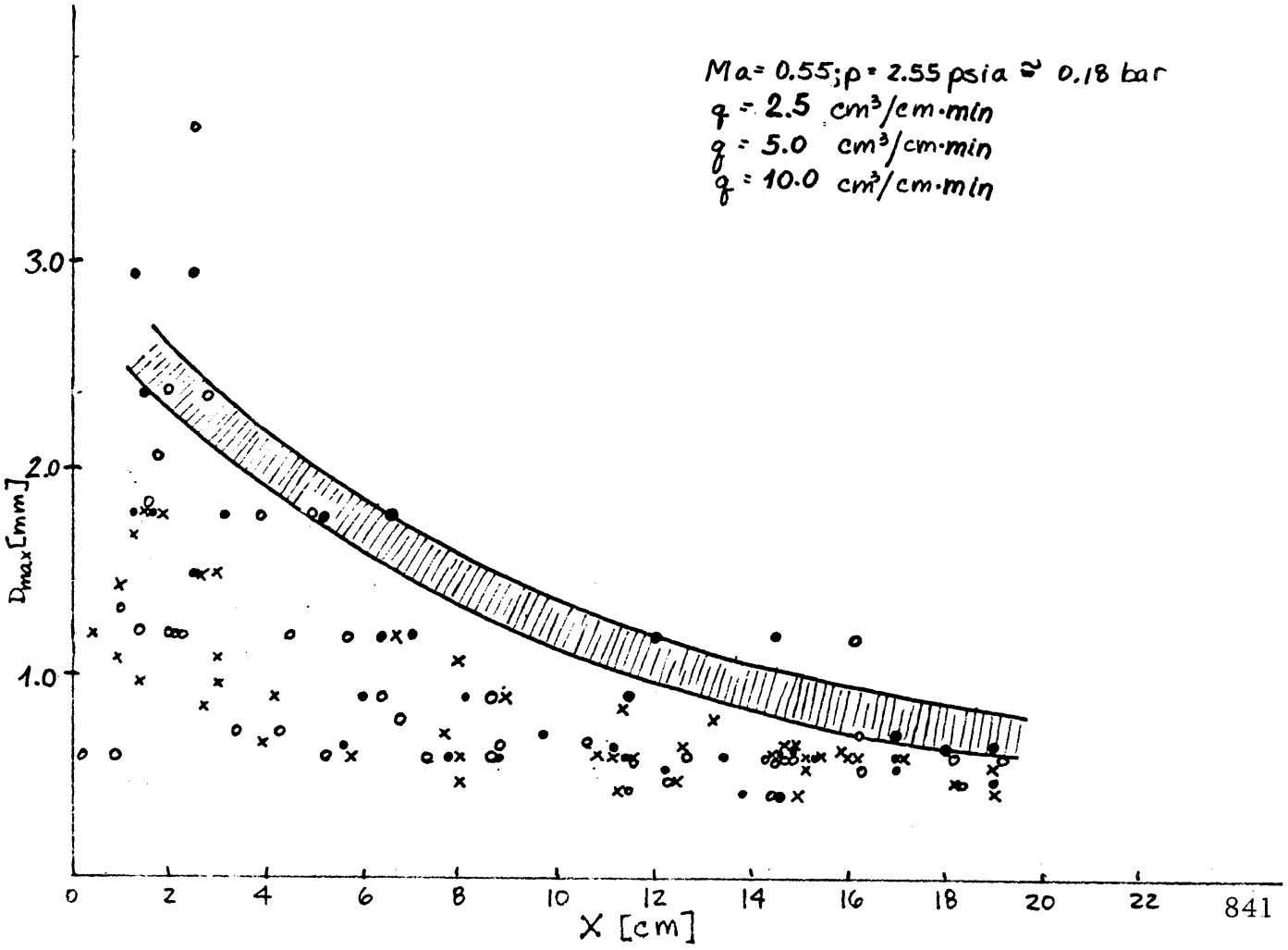

Figure 15 - Maximum Droplet Size as a Function of the Distance From the Trailing Edge, M = 0.55

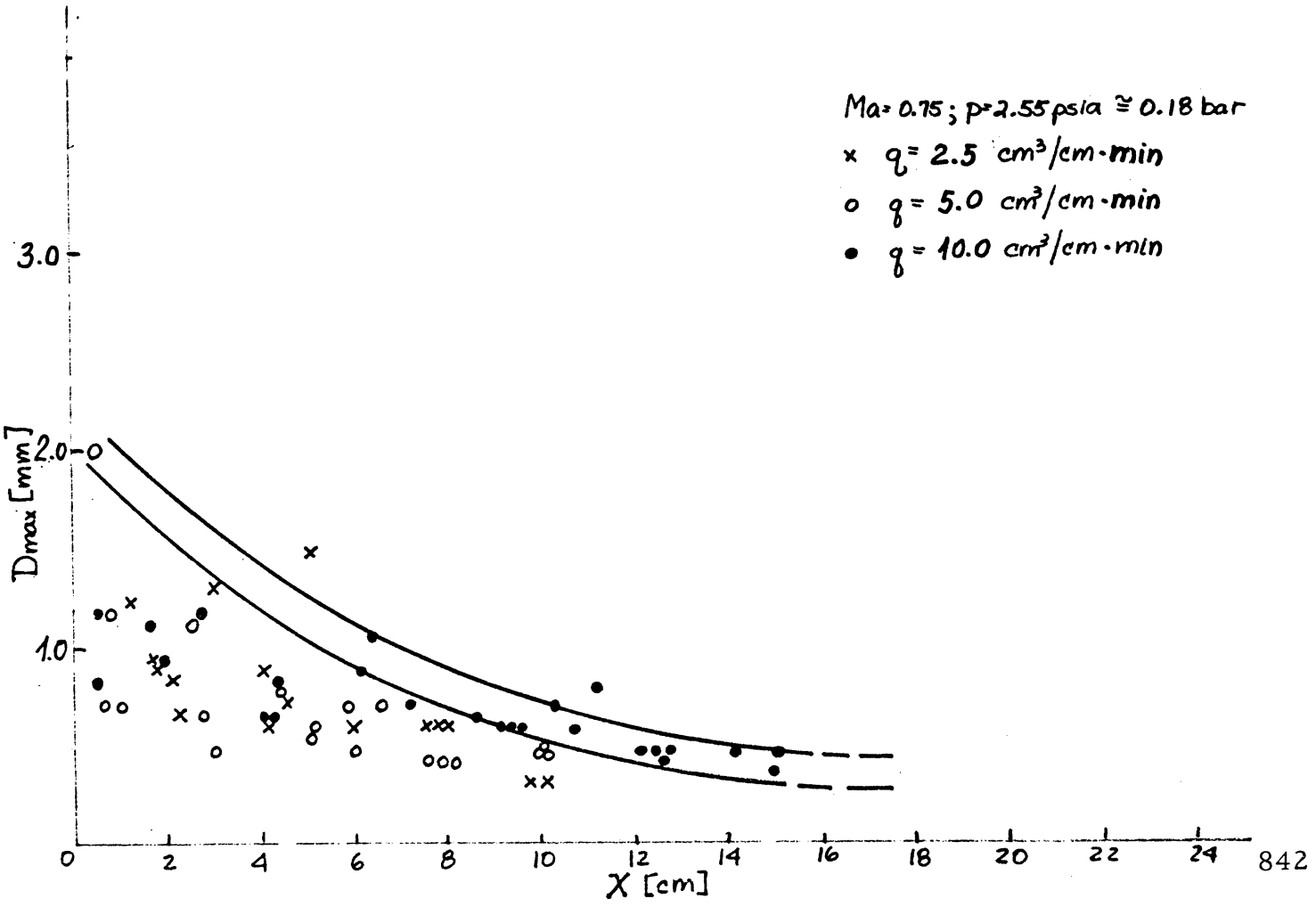

842

Figure 16 - Maximum Droplet Size as a Function of the Distance From the Trailing Edge, M = 0.75

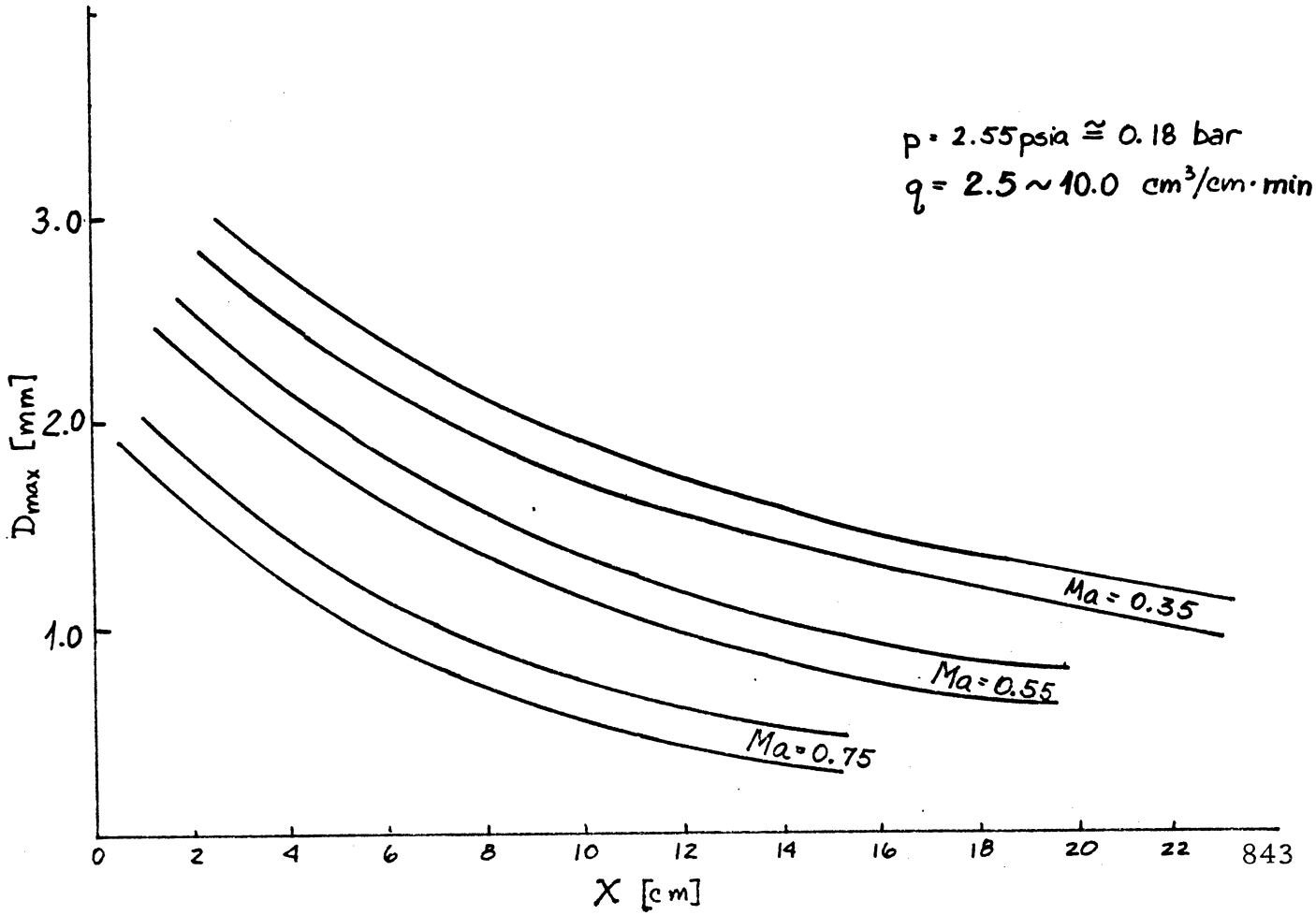

Figure 17 - Maximum Droplet Size as a Function of the Distance From the Trailing Edge at three Mach Numbers

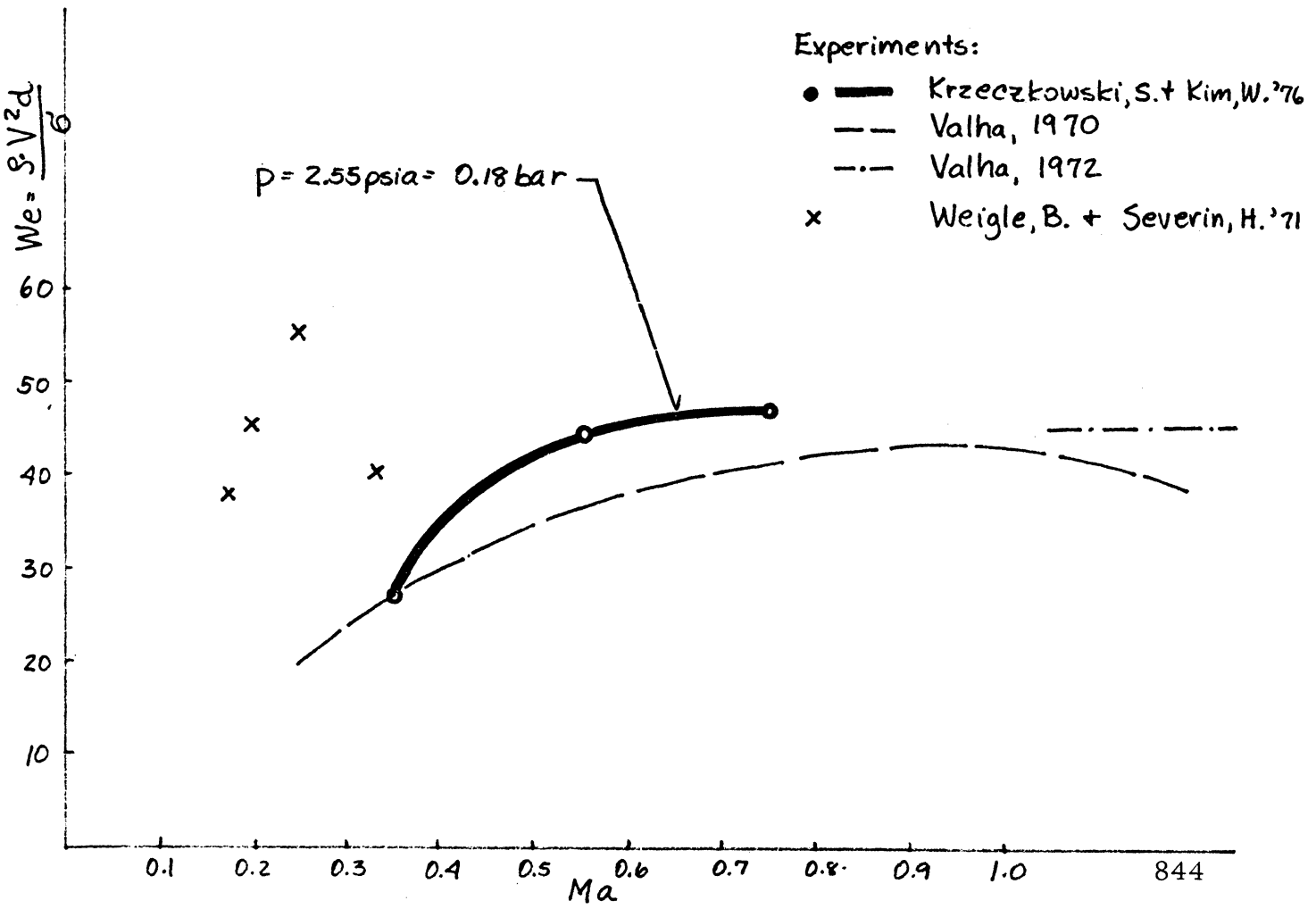

Figure 18 - The Weber Number of Maximum Droplets for Downstream From the Trailing Edge

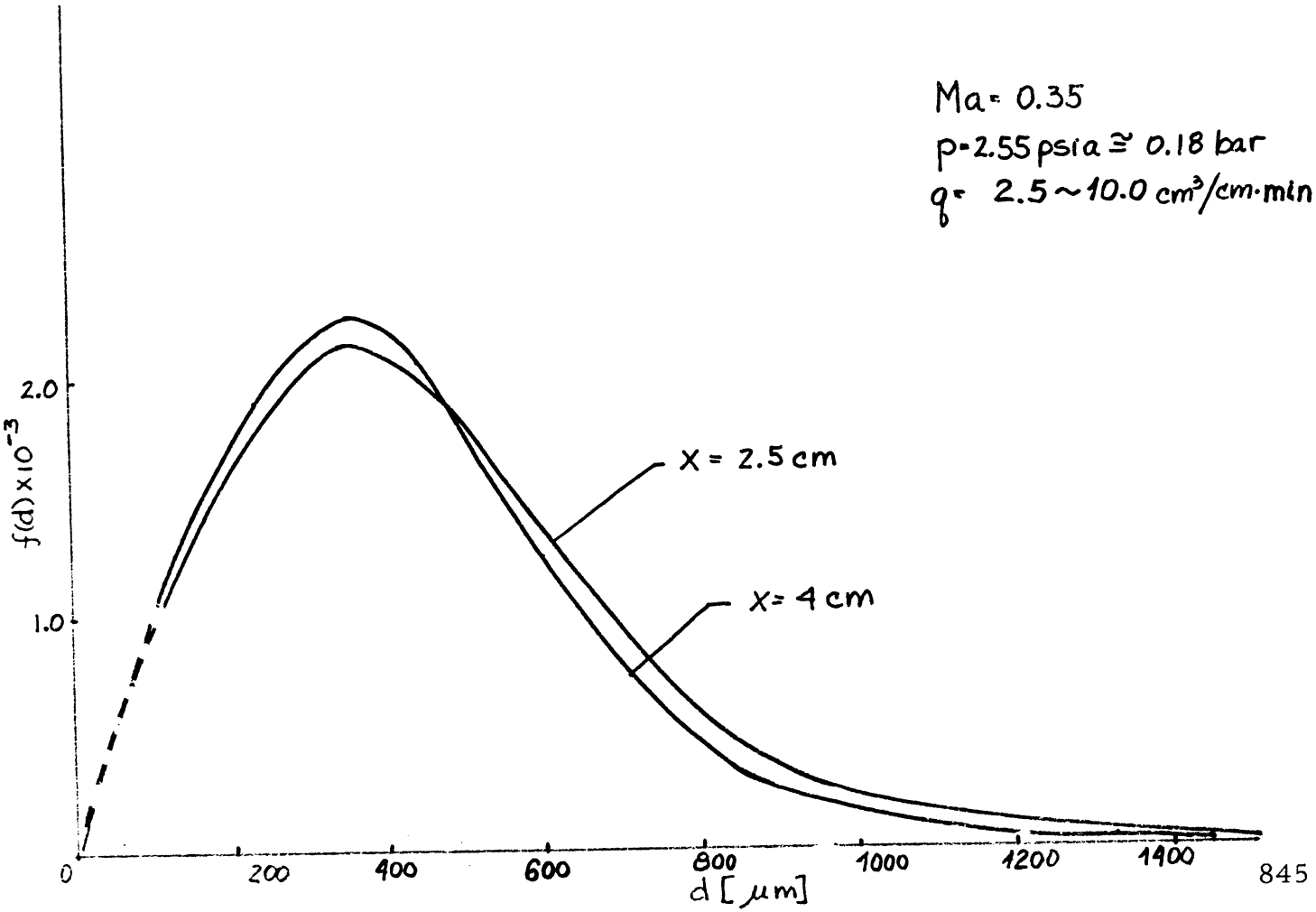

Figure 19 - Droplet Size Distribution Function at M = 0.35, X = 2.5 cm and X = 4.0 cm.

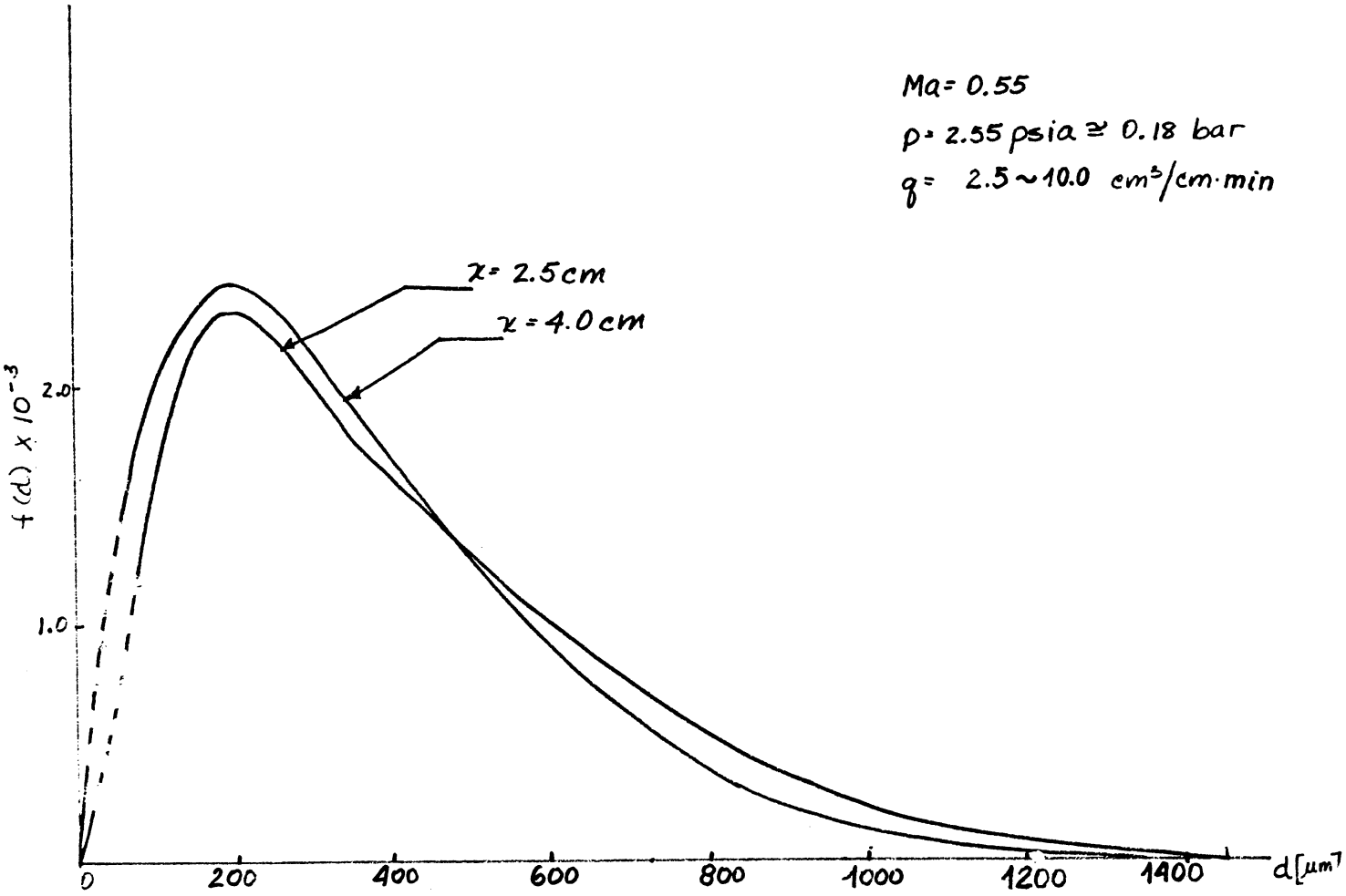

Figure 20 - Droplet Size Distribution Function at M = 0.55, X = 2.5 cm and X = 4.0 cm.

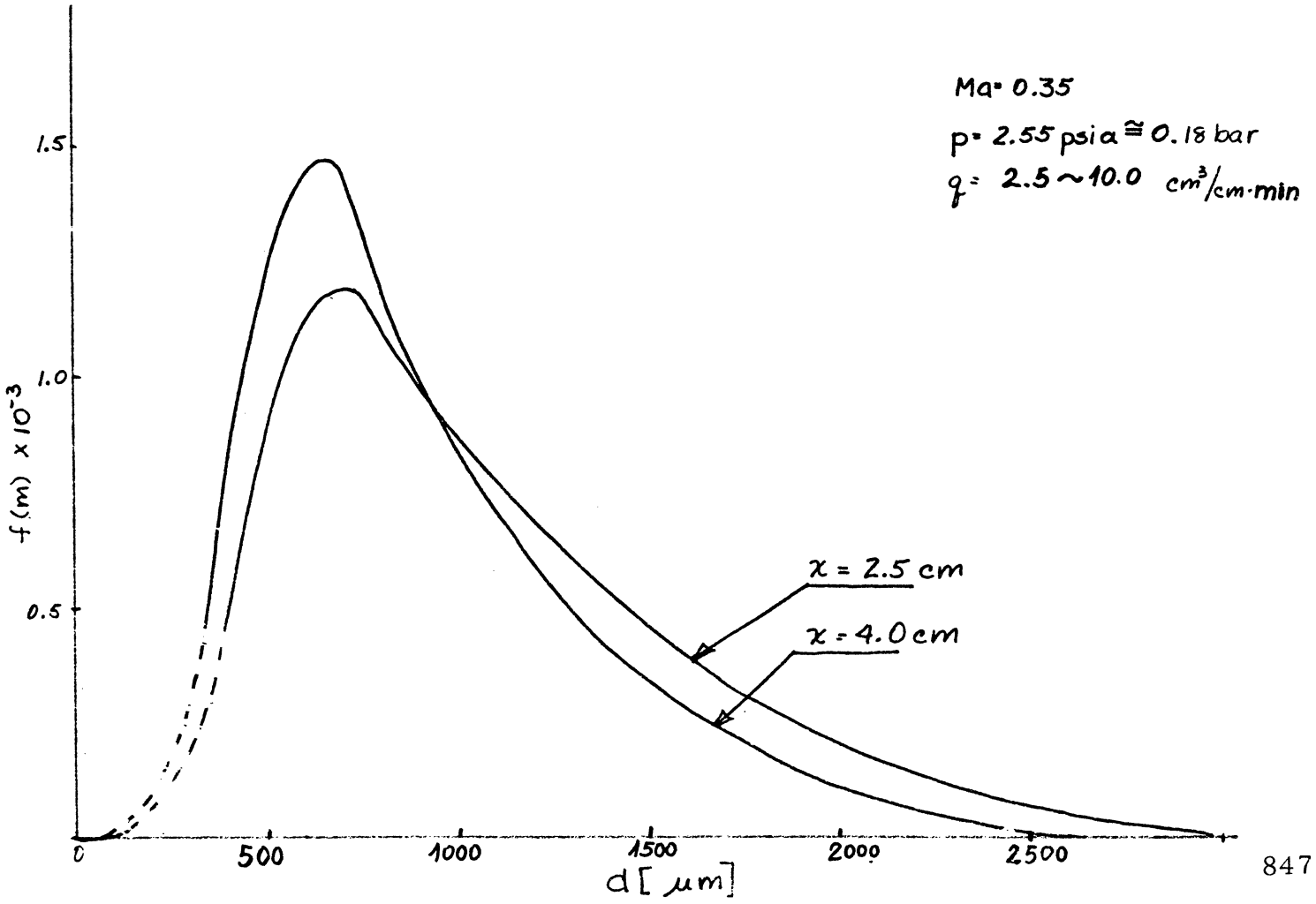

Figure 21 - Droplet Mass Distribution Function at M = 0.35, X = 2.5 cm and X = 4.0 cm

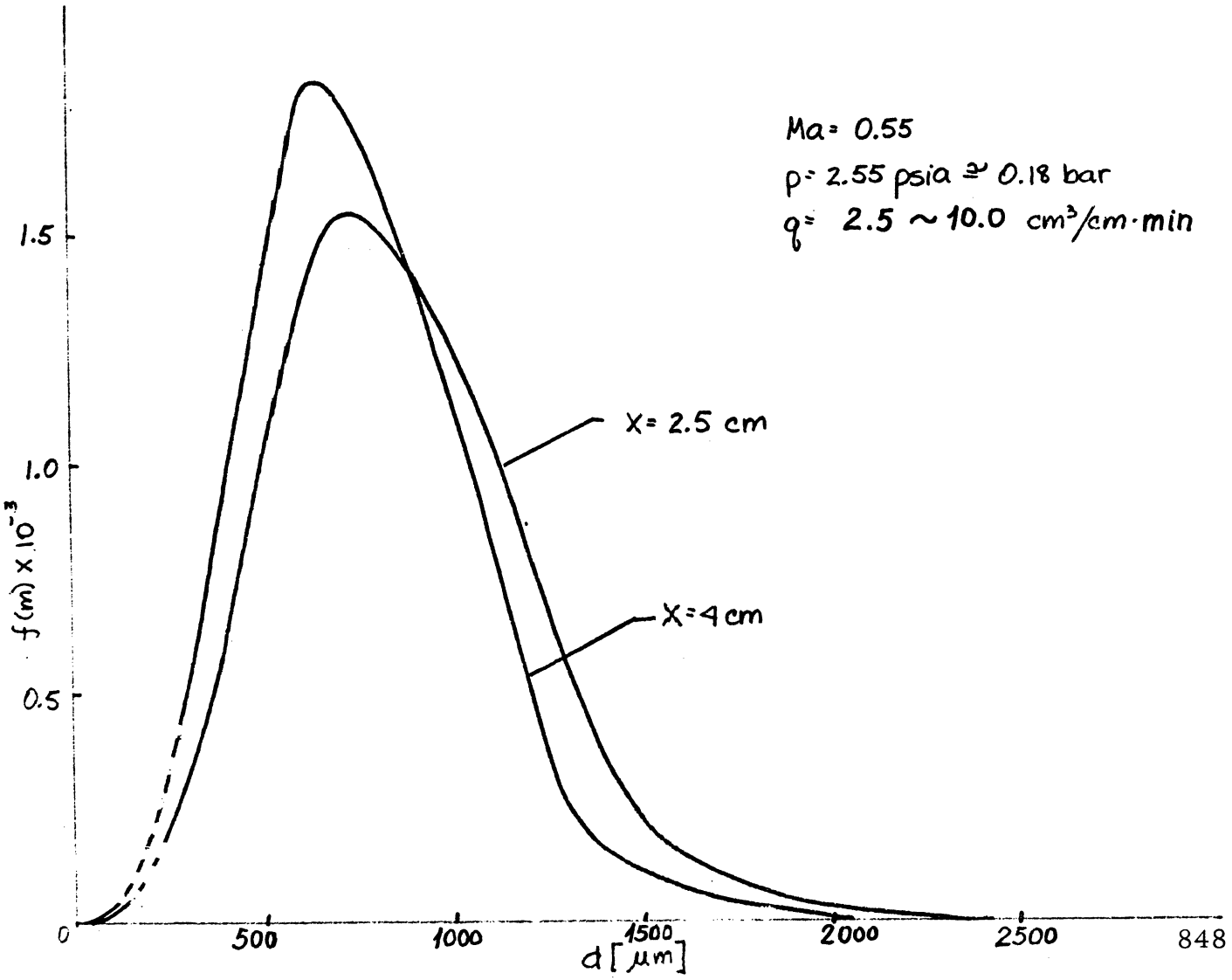

Figure 22 - Droplet Mass Distribution Function at M = 0.55, X = 2.5 cm and X = 4.0 cm.